Automatic Control of the Skylab Astronaut Maneuvering Research Vehicle

T. B. MURTAGH,* C. E. WHITSETT,† M. A. GOODWIN,‡ AND J. E. GREENLEE§
NASA Johnson Space Center, Houston, Texas

The two automatic control modes of the Astronaut Maneuvering Research Vehicle (AMRV) are analyzed: the Control Moment Gyro (CMG) and the Rate Gyro (RG). The AMRV is an autonomous maneuvering unit which translates and rotates the pilot by means of hand-controller input commands. The CMG normal operation, desaturation, and cage/lock dynamics are described in terms of a typical AMRV mass property configuration. No propellant is used for normal operation in the CMG mode, and the maximum rotation rate is 5°/sec about each AMRV axis. The RG attitude maneuvering and limit cycle submode dynamics are described in terms of the same AMRV mass property configuration. In the RG mode, attitude and attitude rate are maintained within limits of ±4° and ±2°/sec, respectively; the maximum rotation rate is 20°/sec about each AMRV axis. Translational maneuvering is identical in either mode, with linear velocities normally not exceeding 0.5 fps.

Introduction

THE purpose of Skylab experiment M509 is to obtain operational experience and engineering/human performance data in a zero gravity environment by using a test bed maneuvering unit. This test bed, the Astronaut Maneuvering Research Vehicle (AMRV), depicted in Fig. 1, was flown inside the Skylab Orbital Workshop (OWS) to avoid the risks and constraints of extravehicular activity (EVA), yet retain the significant characteristics of orbital EVA. The habitable volume of the OWS is sufficient to allow the capabilities and limitations of manned maneuvering to be evaluated in a systematic manner and documented in a laboratory environment. Gaseous nitrogen is used as the propellant to ensure compatibility with the OWS cabin atmosphere.

The AMRV is an autonomous maneuvering unit which translates and rotates the pilot by means of hand-controller input commands. The translational hand-controller (THC) and rotational hand-controller (RHC) are located on the AMRV left and right arm supports, respectively (Fig. 1). The AMRV has four independent control modes which are used to evaluate each of four potential maneuvering unit concepts. The pilot selects among these modes by using a rotary switch located on the AMRV left arm support. The direct mode uses 14 fixed-position backpack thrusters independently selected for translational or rotational maneuvering or both without automatic attitude stabilization (Fig. 2). The backpack is referred to as the Automatically Stabilized Maneuvering Unit (ASMU). The Rate Gyro (RG) mode provides automatic attitude stabilization through rate gyro sensors, control electronics, and reaction control jets with two submodes: attitude maneuvering (proportional rate command input through the RHC) and limit cycle (attitude hold). The Control Moment Gyro (CMG) mode provides rotational maneuvering by means of angular momentum transfer from CMG gimbal activity. CMG torquing commands are generated by RHC displacement from a neutral position. Attitude is automatically maintained without a deadband when the RHC is in a neutral position. During normal operation, no propellant is used for rotational maneuvering or stabilization. The ASMU thrusters provide the necessary torque to desaturate any CMG which has reached an operational limit. Acceleration command translational control is used for the direct, RG, and CMG operating modes with inputs from the THC. The Hand-Held Maneuvering Unit (HHMU) mode uses a hand-held thruster unit actuated by trigger deflection. The unit is manually positioned with respect to the pilot/ASMU center of mass to obtain translation or rotation. The ASMU provides propellant and instrumentation for the HHMU mode.

The purpose of this paper is to document the preflight analysis program which contains the mathematical models of the AMRV control systems. The mathematics and detailed analysis presented in this paper supplement the functional description of the CMG and RG operating modes presented in Ref. 1.

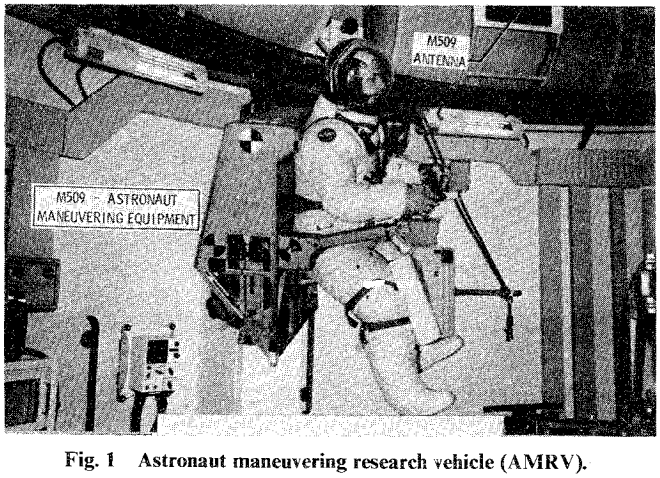

Fig. 1 Astronaut maneuvering research vehicle (AMRV).

Received July 9, 1973; presented at the AIAA Guidance and Control Conference, Key Biscayne, Fla., August 20–22, 1973; revision received November 19, 1973.

Index category: Spacecraft Attitude Dynamics and Control.

* Analysis Co-Investigator, Mission Planning and Analysis Division. Member AIAA.

† Major, U.S. Air Force; also Principal Investigator, U.S. Air Force, Space and Missile System Organization Operating Location. Member AIAA.

‡ Mathematician, Mission Planning and Analysis Division.

§ Mathematician, Computation and Analysis Division. Member AIAA.

ASMU/CMG Dynamics

Rigid Body Equations of Motion

The concept of rigid body is more of a mathematical approximation than a physical reality. The physical reality is a deformable body of finite dimensions which, in effect, possesses an infinite number of degrees of freedom. The mathematical approximation is that body deformations are small compared to motions of the body as a whole and that the distance between any pair of particles in the body is constant. A rigid body can be shown

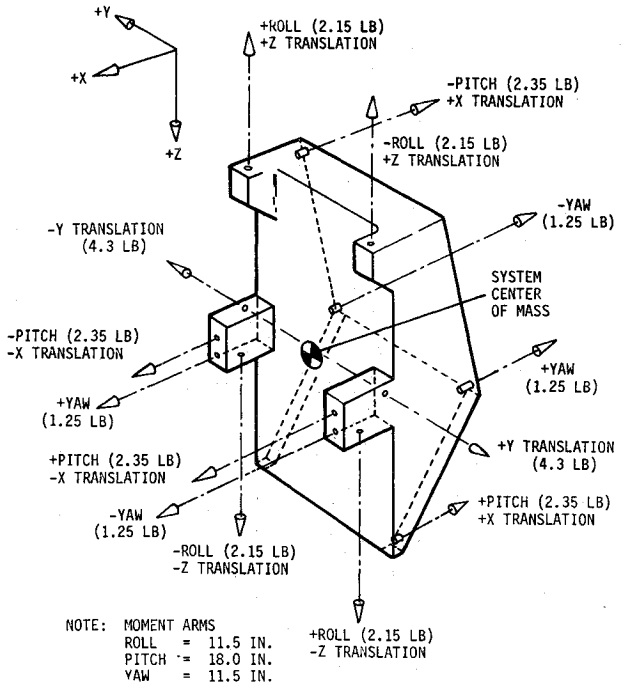

Fig. 2 ASMU thruster location and size.

to possess only six degrees of freedom. The pilot/ASMU system is assumed to be a rigid body. Although this is obviously not true for the human body, the effects of this rigid body assumption on the actual pilot/ASMU dynamic response are the subject of the orbital experiment. This study analyzes the ideal response as a basis for comparison with actual flight results. The translational motion of the center of mass of this system is the same as the translational motion of a particle of mass which is equal to the pilot/ASMU mass and which is acted upon by the same forces as the pilot/ASMU system. The general rotational equations of motion can be written as[2]

$$\bar{M} = I\dot{\bar{\omega}} + \bar{\omega} \times (I\bar{\omega}) \tag{1}$$

In this equation, I is the inertia tensor of the pilot/ASMU system with respect to the center of mass of that system; $\bar{\omega}$ and $\bar{M}$ represent the angular velocity and total external moment vectors, respectively. The computation of the pilot/ASMU mass properties (inertia tensor and location of the pilot/ASMU center of mass with respect to the ASMU center of mass) is discussed in detail in Ref. 3. In the RG operating mode of the AMRV, $\bar{M}$ is generated by backpack (ASMU) thruster activity. In the CMG mode, $\bar{M}$ is generated by angular momentum exchange between the ASMU and the CMG assembly (CMGA), backpack thruster activity, or both. Gravitational moments are also present, but are negligible in comparison with ASMU- or CMG-generated moments.

CMG Moments

The angular momentum exchange between the pilot/ASMU system and the CMGA can be represented by

$$\bar{M}_T = \dot{\bar{H}} + \bar{\omega} \times \bar{H} + \sum_{i=1}^{3} [\dot{\bar{H}}_G + \bar{\omega} \times \bar{H}_G] \tag{2}$$

In this equation, $\bar{M}_T$ is the moment vector due to ASMU thruster activity, $\bar{H}$ is the angular momentum of the pilot/ASMU system, and $\bar{H}_G$ is the angular momentum of a CMG. The summation notation indicates the existence of three CMG's, one for each AMRV axis. The first two terms on the right-hand side of Eq. (2) are the terms on the right-hand side of Eq. (1). Thus, the total external moment vector, $\bar{M}$, becomes

$$\bar{M} = \bar{M}_T - \bar{M}_G \tag{3}$$

Table 1 CMG performance data

Parameter	Value	Units
Number of CMG's	3 pair	...
Degrees of freedom per CMG	1	...
Gimbal caging position	Null ± 0.25	deg
Gimbal freedom	±60	deg
ASMU command rates		
Maximum	5	deg/sec
Threshold	0.2	deg/sec
Sensitivity	1	volt/deg/sec
Output torque (max)	21	ft-lb
Drift rate (max)	0.1	deg/sec
Wheel spin speed (max)	22,500	rpm
Stored momentum (max)	±1.7	ft-lb-sec
Wheel rotation times		
Spin-up	20	min
Life	500	hr
Spin-down	60	min

where the CMG moment vector, $\bar{M}_G$, is given by

$$\bar{M}_G = \sum_{i=1}^{3} [\dot{\bar{H}}_G + \bar{\omega} \times \bar{H}_G] \tag{4}$$

The CMG angular momentum in the ASMU body-fixed coordinate system is[4]

$$\sum_{i=1}^{3} \bar{H}_G = 2H_W[\sin\alpha_X \hat{i} + \sin\alpha_Y \hat{j} + \sin\alpha_Z \hat{k}] \tag{5}$$

In this equation H_W is a CMG wheel angular momentum (two wheels per CMG), and α_X, α_Y, and α_Z are the CMG gimbal angles for the roll, pitch, and yaw axes; $\hat{i}$, $\hat{j}$, and $\hat{k}$ are unit vectors along the X, Y, and Z ASMU body-fixed coordinate axes (Fig. 2). If the angular velocity $\bar{\omega}$ is defined as

$$\bar{\omega} = \omega_X \hat{i} + \omega_Y \hat{j} + \omega_Z \hat{k} \tag{6}$$

then, from Eqs. (5) and (6), Eq. (4) becomes

$$\bar{M}_G = 2H_W[M_{GX}\hat{i} + M_{GY}\hat{j} + M_{GZ}\hat{k}] \tag{7}$$

where

$$M_{GX} = \dot{\alpha}_X \cos\alpha_X + \omega_Y \sin\alpha_Z - \omega_Z \sin\alpha_Y \tag{8a}$$

$$M_{GY} = \dot{\alpha}_Y \cos\alpha_Y + \omega_Z \sin\alpha_X - \omega_Z \sin\alpha_Z \tag{8b}$$

$$M_{GZ} = \dot{\alpha}_Z \cos\alpha_Z + \omega_X \sin\alpha_Y - \omega_Y \sin\alpha_X \tag{8c}$$

CMG Gimbal Dynamics

The rationale for the selection of the CMG control laws is provided in Ref. 4; a discussion and analysis of AMRV stability with CMG's are contained in Ref. 5. The CMG control system operational diagram is presented in Fig. 3. With this figure, the simulated nonlinear second-order differential equation describing the CMG gimbal angle dynamics becomes

$$\ddot{\alpha}_i = [2H_W \omega_i - K_T \dot{\beta}_i - K_R \dot{\alpha}_i - K_T K_C \alpha_i] \cos\alpha_i / 2I_G \tag{9}$$

In this equation, $i = 1, 2, 3$ corresponds to the AMRV roll, pitch, and yaw axes, respectively ($\alpha_1 = \alpha_X$; $\alpha_2 = \alpha_Y$; and $\alpha_3 = \alpha_Z$).

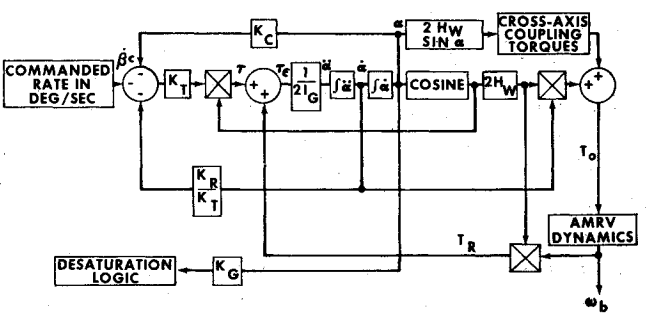

Fig. 3 CMG control system operational diagram.

Table 2 CMG control system parameters

Parameter	Value
K_R	0.0202 ft-lb/rad/sec
K_C	20.6 v/rad
K_T	0.0387 ft-lb/v
K_G	0.0833 v/deg
I_G	13.35×10^{-4} slug-ft^2
H_W	1.05 ft-lb-sec

Specific CMG performance data are presented in Table 1; the CMG wheel angular momentum and gimbal inertia, H_W and I_G, are listed in Table 2. The commanded rate, $\dot{\beta}_i$, cannot exceed 5°/sec for each AMRV axis. The CMG control system gains (K_T, K_R, K_C) are listed in Table 2; for CMG normal operation and desaturation, $K_C = 0$.

CMG Control System

Normal Operation

The CMG normal operation can best be described by considering Eqs. (1, 3, 7–9). Assume zero initial conditions for the CMG gimbal angles and rates, and assume zero initial pilot/ASMU angular velocity. Let $\dot{\beta}_1 = 2°$/sec and $\dot{\beta}_2 = \dot{\beta}_3 = 0$ (this corresponds to a 2°/sec roll command). Further, assume that the pilot/asmu inertia tensor, I, is diagonal with $I_{XX} = I_{YY} = I_{ZZ}$. This removes all dynamic cross-coupling, and, for the assumed roll command, Eq. (1) becomes

$$\dot{\omega}_X = M_X/I_{XX} \tag{10}$$

Since there is no dynamic cross-coupling or thruster activity [$\bar{M}_T = 0$ in Eq. (3)], the total moment about the roll axis is

$$M_X = -M_{GX} = -2H_W \dot{\alpha}_X \cos\alpha_X \tag{11}$$

Combining Eqs. (10) and (11) yields

$$\dot{\omega}_X = -(2H_W/I_{XX})\dot{\alpha}_X \cos\alpha_X \tag{12}$$

For the assumptions made, Eq. (9) simplifies to

$$\ddot{\alpha}_X = [2H_W \omega_X - K_T\dot{\beta}_1 - K_R\dot{\alpha}_X]\cos\alpha_X/2I_G \tag{13}$$

Equations (12) and (13) are a coupled set of second-order differential equations. With the positive roll command and the assumed zero initial conditions, α_X begins to decrease [$\ddot{\alpha}_X$ in Eq. (13) is initially negative]. As α_X decreases, $\dot{\alpha}_X$ is negative, and a positive moment is generated via Eq. (11). This CMG moment creates a positive angular acceleration, $\dot{\omega}_X$, about the roll axis. The CMG gain, K_T, is chosen such that, when the commanded rate is achieved ($\omega_X = \dot{\beta}_1 = 2°$/sec), then

$$2H_W\omega_X - K_T\dot{\beta}_1 = 0 \tag{14}$$

When the actual rate, ω_X, and the commanded rate, $\dot{\beta}_1$, are equal, the gimbal rate, $\dot{\alpha}_X$, is zero. When the command is removed ($\dot{\beta}_1 = 0$), the gimbal acceleration, $\ddot{\alpha}_X$, reverses sign, and, consequently, the moment reverses sign. This sequence of events then drives the actual rate, ω_X, to zero in order to stabilize the AMRV roll attitude.

Desaturation

For the simplified dynamic situation considered in the previous section, Eq. (11) is based on the assumption that the total moment is created by the roll axis CMG; in other words, no roll thrusters are activated. If a given CMG gimbal angle exceeds an operational limit, however, backpack thrusters are activated in order to drive the gimbal within the operational limit. This process is called desaturation. With the present CMG control system design parameters, the desaturation sequence will begin for $|\alpha_i| \geqq 53°$ and terminate for $|\alpha_i| \leqq 48°$. During desaturation, the rate command is not inhibited; therefore, the total moment vector is given by Eq. (3). During the desaturation process, the gyro can be gimbaled to mechanical stops at $\pm 60°$. Impact into the gimbal stops at gimbal rates up to ± 15 rad/sec does not cause functional failure. The design philosophy associated with the CMG system configuration, gimbal limits, mechanical stops, and saturation is contained in Ref. 6. The gimbal mechanical stops are simulated by testing the absolute value of the gimbal angle. If this value exceeds 60°, the gimbal rate and acceleration are instantaneously set to zero. Integration of Eq. (9) proceeds as before. Eventually the gimbal acceleration changes sign, the gimbal angle is driven less than 60°, and the ASMU thrusters complete the desaturation process. The thrusters continue to operate even though the gimbals are against the mechanical stops.

Cage and Lock

The AMRV operating modes are selected by using a rotary switch located beside the THC on the left arm of the AMRV. When the mode select switch is rotated from "CMG mode" to any other mode, an automatic caging sequence takes place. The CMG caging logic is as follows. If

$$K_G K_C \alpha_i \geqq 18 \tag{15}$$

then a negative rotation command is issued to the ASMU thrusters. If

$$K_G K_C \alpha_i \leqq -18 \tag{16}$$

then a positive rotation command is issued to the ASMU thrusters. Activation of thrusters according to either Eq. (15) or (16) corresponds to initiating the coarse cage sequence. Based on the values of K_G and K_C (see Table 2) the coarse cage initiates for gimbal angles greater than 10.8°. If neither Eq. (15) nor (16) is true, no rotation commands are issued to the backpack thrusters, and the fine cage sequence is begun. The fine cage initiates for gimbal angles less than 10.8°. For the fine cage sequence, electronic feedback is actuated within the CMGA to torque the gimbals toward zero gimbal angle. During the coarse caging sequence for each CMG, the rate command for that axis is inhibited ($\dot{\beta}_i = 0$); the rate command inhibit is removed during CMG fine cage. The requirement for a successful gimbal lock is that the gimbal angle be less than 1° for at least 0.2 sec.

If the mode select switch is rotated back to the "CMG mode" from any other mode, then each CMG is unlocked and uncaged, provided the AMRV angular velocity about the respective axis is less than 10°/sec. If the rate about a particular axis exceeds 10°/sec when mode switching occurs, that axis is automatically switched to the rate gyro mode until the rate is reduced to less than 10°/sec. Rate commands for the axis affected are inhibited until the rate is reduced.

Fine Cage Analytic Model

During the fine cage sequence, the CMG gimbal angle is less than 10.8°. This fact allows the conversion of Eq. (9) to a linear second-order differential equation by setting $\cos\alpha_i \approx 1$. Therefore, Eq. (9) becomes

$$J_G\ddot{\alpha}_i = H\omega_i - K_T\dot{\beta}_i - K_R\dot{\alpha}_i - K_T K_C \alpha_i \tag{17}$$

where

$$H = 2H_W \tag{18}$$

and

$$J_G = 2I_G \tag{19}$$

Equation (17) is almost in the form of an unforced damped harmonic oscillator, the solution to which is known. Some additional observations concerning the ω_i term indicate how Eq. (17) can be converted to the desired form. Assume that no thruster commands are issued during the fine cage sequence ($\dot{\beta}_i = 0$) so that the only torques on the pilot/ASMU system are from CMG gimbal activity. Further assume that the pilot/ASMU inertia tensor is diagonal so that [see Eq. (12)]

$$J_B\dot{\omega}_i = -H\dot{\alpha}_i \tag{20}$$

This equation can be integrated to provide a relationship between ω_i and α_i. The parameter J_B in Eq. (20) represents a diagonal element of the pilot/ASMU inertia tensor. Integrating Eq. (20) yields

$$\omega_i = \omega_o - (H/J_B)(\alpha_i - \alpha_o) \tag{21}$$

In Eq. (21) ω_o and α_o are initial conditions for the pilot/ASMU angular velocity and CMG gimbal angle, respectively. Substituting Eq. (21) into Eq. (17) yields an equation in the form of an unforced damped harmonic oscillator,[7] that is

$$\ddot{\alpha}_i + 2\zeta\omega_N \dot{\alpha}_i + {\omega_N}^2 \alpha_i - K = 0 \tag{22}$$

In this equation, K is a constant, ζ is the damping ratio, and ω_N is the undamped natural frequency. These parameters are defined by

$$K = \frac{1}{J_G}\left[H\omega_o + \frac{H^2\alpha_o}{J_B}\right] \tag{23a}$$

$$\zeta = \frac{K_R}{2}\left[J_G\left(K_T K_C + \frac{H^2}{J_B}\right)\right]^{-1/2} \tag{23b}$$

$$\omega_N = \left[\frac{1}{J_G}\left(K_T K_C + \frac{H}{J_B}\right)\right]^{1/2} \tag{23c}$$

For the values of the CMG control system parameters presented in Table 2, the damping ratio is less than unity. This corresponds to an under-damped system, and the transient solution to Eq. (22) takes the form

$$\alpha_i(t) = e^{-\zeta\omega_N t}\{C_1 \cos[\omega_N(1-\zeta^2)^{1/2}t] + C_2 \sin[\omega_N(1-\zeta^2)^{1/2}t]\} + K/{\omega_N}^2 \tag{24}$$

The constant $\omega_N(1-\zeta^2)^{1/2}$ is the damped natural frequency, and C_1, C_2 are constants of integration to be determined from initial conditions. For $t = 0$, if $\alpha_i = \alpha_o$ and $\dot{\alpha}_i = \dot{\alpha}_o$, then

$$C_1 = \alpha_o - K/{\omega_N}^2 \tag{25}$$

and

$$C_2 = (\dot{\alpha}_o + \zeta\omega_N \alpha_o)/\omega_N(1-\zeta^2)^{1/2} \tag{26}$$

Equation (24) can be used to compute the CMG fine cage dynamic response characteristics.

Rate Gyro Control System

The control logic for the RG operating mode of the AMRV is illustrated in Fig. 4. This logic is used for each of the AMRV roll (ϕ), pitch (θ), and yaw (ψ) rotational commands.

The RG attitude maneuvering submode operates in the following functional manner. Rotational commands are generated by deflecting the RHC from the null position. The commanded angular rate is proportional to the angular deflection of the RHC. The commanded rate is compared with the actual rate (from the rate gyro sensors) to produce a rate error signal for each axis (roll, pitch, and yaw). The rate error signal is then passed through a rate modulator which produces commands to the thruster select logic for each axis.[1] Threshold logic in the rate modulator provides for a smooth transition to the commanded rate.

In the limit cycle submode, input commands from the RHC are effectively zero. The AMRV rate and attitude control is

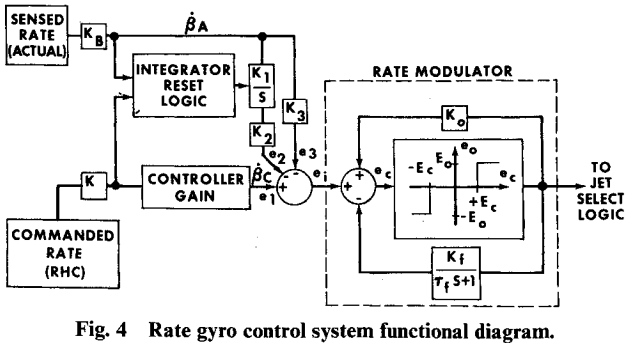

Fig. 4 Rate gyro control system functional diagram.

Table 3 Rate gyro performance data

Parameter	Value	Units
Number of rate gyros	3	...
Degrees of freedom per gyro	1	...
Gimbal freedom	±2	deg
Input sensitivity	0.1	v/deg/sec
Output levels		
Maximum	50	deg/sec
Threshold	0.01	deg/sec
Drift rate	0.02	deg/sec
Null uncertainty	±3.5	mv
ASMU command rate (max)	20	deg/sec
Wheel spin speed	24,000	rpm
Wheel spin-up time	10	sec

Table 4 Rate gyro control system parameters

Parameter	Value
K_B	1 v/v
K_D	2.83 vdc/vrms
K_1	10 v/v-sec
K_2	0.796 v/v
K_3	14.9 v/v
K_0	0.45 v/v
K_f	7.2 v/v
τ_f	0.3 sec

based on the rate gyro sensor outputs. An attitude reference is established when the RHC is released and the rate is automatically reduced below 4°/sec. A limit cycle deadband of ±2°/sec and ±4° is produced by the application of the sum of attitude and attitude rate errors to the rate modulator. This in turn forms a series of on/off commands to the jet select logic.

The input to the simulated rate modulator is given by

$$e_i = 0.1K_3(\dot{\beta}_C - \dot{\beta}_A) - K_2\Delta\xi \tag{27}$$

where $\dot{\beta}_C$ and $\dot{\beta}_A$ are the commanded and actual rates and $\Delta\xi$ is the attitude error. Threshold logic is dependent upon the parameter $e_C(t)$, defined by

$$e_C(t) = e_i + K_o E_o - K_f E_o(1 - e^{-t/\tau_f}) \tag{28}$$

Specific rate gyro performance data are presented in Table 3; the rate gyro control system gains and time constant, τ_f, are listed in Table 4. If

$$-3 < e_C(t) < 3 \tag{29}$$

then $E_o = 0$, implying no rotational commands to the jet select logic. If

$$e_C(t) \geqq 3 \tag{30}$$

then $E_o = +1$, implying a positive rotational command to the jet select logic. If

$$e_C(t) \leqq -3 \tag{31}$$

then $E_o = -1$, implying a negative rotational command. Positive rotational commands imply clockwise (CW) rotation (from the pilot's viewpoint), and negative rotational commands imply counterclockwise (CCW) rotation.

Results and Analysis

The mass property data for Figs. 5 and 8 are presented in Table 5 and represent a 150 lb unsuited pilot with the ASMU. Background on the computation of mass property data for the pilot/ASMU system is contained in Ref. 3. The parameters ΔX, ΔY, ΔZ are components of the vector locating the center of mass of the pilot/ASMU system with respect to the ASMU center of mass.

Figure 5 illustrates typical CMG gimbal angles and pilot/ASMU body rates resulting from a digital simulation of a series

Table 5 Mass property data for 150-lb pilot plus ASMU

Parameter	Value
I_{xx}	17.8 slug-ft^2
I_{yy}	20.0 slug-ft^2
I_{zz}	10.9 slug-ft^2
I_{xy}	0.3 slug-ft^2
I_{xz}	-2.1 slug-ft^2
I_{yz}	-0.5 slug-ft^2
ΔX	-1.156 in.
ΔY	0.179 in.
ΔZ	-0.190 in.
M	405.3 lb

of commands which included CMG normal, desaturation, cage/lock, and uncage/unlock operations. A realistic inertia tensor introduced dynamic cross-coupling effects. All commands were for the AMRV roll axis, but dynamic cross-coupling produced moments about each axis [see Eq. (8)]. The first command was a 2°/sec roll for 3 sec. In about 0.4 sec this body rate was achieved. The corresponding CMG roll gimbal angle was $-17.2°$. Dynamic coupling between the roll and yaw axes ($I_{xz} = -2.1$ slug-ft^2) produced a yaw gimbal angle of 2.14°. The smaller coupling between the roll and pitch axes ($I_{xy} = 0.3$ slug-ft^2) produced a pitch gimbal angle of 0.87°. Because the CMG gimbals did not saturate during this period, no thrusters were activated. The effect of cross-coupling on the body rates was negligible.

A 1-sec coast followed. Both the CMG gimbal angles and the AMRV body rates were quickly reduced to zero. Next, a minus (CCW) 5°/sec roll was commanded for 3 sec. The CMG roll gimbal angle had a value of 53.3° after 0.3 sec (gimbal saturation). The negative roll thrusters came on for 0.18 sec (desaturation). The value of the roll gimbal angle was then 47.8° (desaturation complete). The X-axis body rate during desaturation exceeded the commanded rate briefly, then settled down to -5.0°/sec. The pitch and yaw CMG gimbal angles caused by cross-coupling stabilized at 2.2° and -4.8°, respectively.

At the end of the subsequent 0.03-sec coast, the CMG roll, pitch, and yaw gimbal angles were 18.05°, 2.23°, and -4.78°, respectively. The corresponding X, Y, and Z body rates were -4.6, -0.004, and 0.07°/sec (roll, pitch, and yaw).

A mode switch to the direct mode was commanded. The ASMU thrusters came on to begin the cage/lock sequence, and the CMG roll gimbal angle was reduced to less than 1° in 0.03 sec. (The 0.2-sec delay before allowing gimbal lock is not presently simulated.) The pitch gimbal locked in 0.05 sec and the yaw gimbal locked in 0.06 sec. A direct mode positive roll was commanded for 1.5 sec, during which the CMG gimbals remained locked. At the end of the time, the X, Y, and Z body rates were 17.38, -0.59, and 3.20°/sec, respectively.

Next, a mode switch was commanded to the CMG mode. Since the angular velocity about the X body axis exceeded 10°/sec, that axis was automatically switched to the rate gyro mode. The negative roll thrusters came on, and, within 0.06 sec, the X, Y, and Z body rates were 9.41, -0.82, and 1.55°/sec, respectively. Uncage/unlock was complete. Then a -3°/sec roll was commanded for 2 sec. The CMG roll gimbal angle saturated after 0.1 sec, and the negative roll thrusters came on. The angle continued to increase until it reached 63.4° (simulated gimbal mechanical stop). It then decreased rapidly and the thrusters shut off (desaturation complete). The thrusters fired for a total of 1.04 sec. At the end of the commanded 2 sec, the roll, pitch, and yaw gimbal angles were -15.44°, -5.39°, and -3.71°, respectively. The corresponding X, Y, and Z body rates were -3.0, 0, and 0°/sec; the body rates had stabilized after about 1.76 sec.

Equation (24) can be used to compute the final value of the gimbal angle during CMG fine cage after the decay of the transient. This final value is calculated by letting time, t, approach infinity so that

$$\alpha_i(\infty) = \alpha_f = K/\omega_N{}^2 \tag{32}$$

Substituting Eqs. (23a) and (23c) into this equation gives

$$\alpha_f/\alpha_o = \frac{H\omega_o/\alpha_o + H^2/J_B}{K_T K_C + H^2/J_B} \tag{33}$$

Inspection of Eq. (33) reveals that certain combinations of ω_o, α_o, and J_B will cause the final value of the CMG gimbal angle to be greater than 1°, so that CMG gimbal lock will not occur. The ratio α_f/α_o is plotted against the ratio ω_o/α_o for two values of J_B in Fig. 6 [the values of K_T, K_C, and H ($= 2H_W$) in Table 2 are assumed]. Note that, if $\alpha_f/\alpha_o = 1$, then the relationship in Eq. (33) is insensitive to J_B. This can be verified in Fig. 6 by observing that for $\alpha_f/\alpha_o = 1$ the lines for J_B intersect. The use of Fig. 6 in predicting CMG gimbal lock is illustrated as follows. Suppose $J_B = 12$ slug-ft^2 and $\omega_o/\alpha_o = 0.6$; then, from Fig. 6, $\alpha_f/\alpha_o = 1.5$. If the initial gimbal angle is 5° and the initial pilot/ASMU angular velocity is

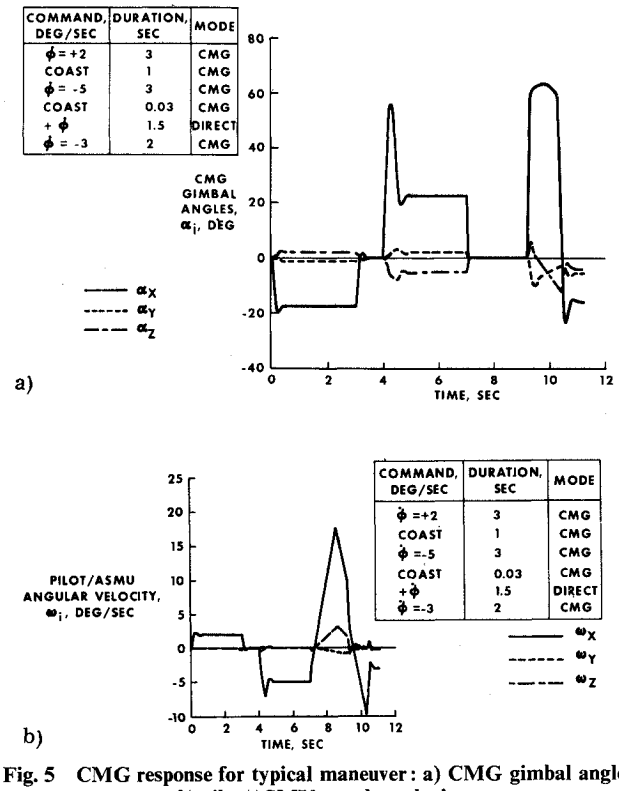

Fig. 5 CMG response for typical maneuver: a) CMG gimbal angles; b) pilot/ASMU angular velocity.

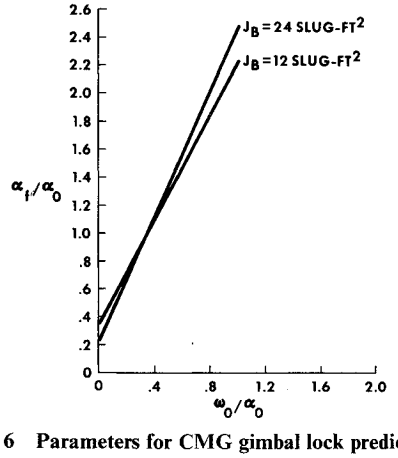

Fig. 6 Parameters for CMG gimbal lock prediction.

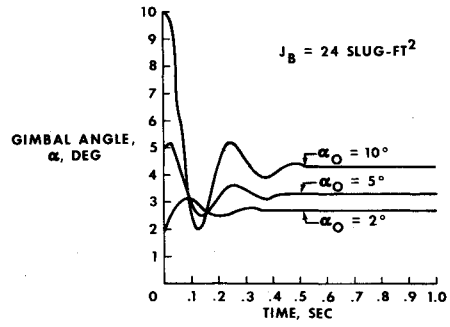

Fig. 7 CMG fine cage analytic response.

3°/sec (that is, $\omega_o/\alpha_o = 0.6$), then, since $\alpha_f/\alpha_o = 1.5$, the final gimbal angle will be 7.5° and CMG gimbal lock will not occur.

Figure 7 illustrates the fine cage analytic response [see Eq. (24)] with an initial pilot/ASMU angular velocity of 1°/sec and with zero initial gimbal angle rate ($\dot{\alpha}_o = 0$). Three different initial conditions were assumed for the gimbal angle ($\alpha_o = 2°$, 5°, and 10°). This figure shows that the period of the unforced damped harmonic oscillator represented by Eq. (22) is 0.2 sec. This explains why the condition for CMG gimbal lock is that the gimbal angle remain less than 1° for at least 0.2 sec. The 0.2-sec tolerance allows time for the initial transient to decay and for the gimbal angle to settle down to its true final value. The final values of the gimbal angles in Fig. 7 can be predicted from Fig. 6.

Simulated AMRV rate gyro mode angular rates are shown in Fig. 8a. The angular rates in the figure are representative of a 150-lb pilot with the ASMU (see Table 5) who, starting from a stationary attitude, actuates the RHC for a maximum angular rate command of 20°/sec about the roll axis. This command is held for 3 sec and then released, so that the system returns to the attitude hold submode. Although 20°/sec is commanded, the rate cuts off at slightly over 18°/sec because of the 2°/sec deadband associated with the rate gyro mode. The rates about the pitch and yaw axes, which are caused by dynamic cross-coupling, are kept within the attitude hold limits according to the rate modulator deadband logic.

Limit cycle data from a typical AMRV translational maneuver are shown in Fig. 8b. The AMRV system is accelerated to 0.34 fps with a 1-sec $+Y$ translational command. This velocity is maintained for 3 sec, and then a 1-sec translation command is given to reduce the velocity to zero. The mass property data are the same as that described in Table 5, and the center of mass offset of -1.16 in. (ΔX) causes rates to build up about the yaw axis during the translational thrust. The data in this figure show how the rate gyro control system keeps these rates within the ± 2°/sec limits, and keeps the attitude angles within the ± 4° limits. In this maneuver the pilot/ASMU system translates 1.37 ft within a total of 5 sec.

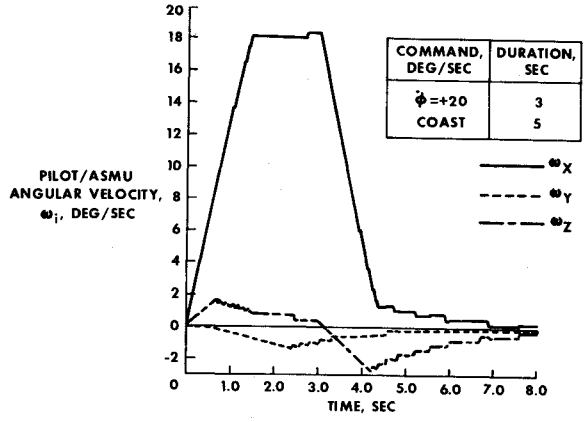

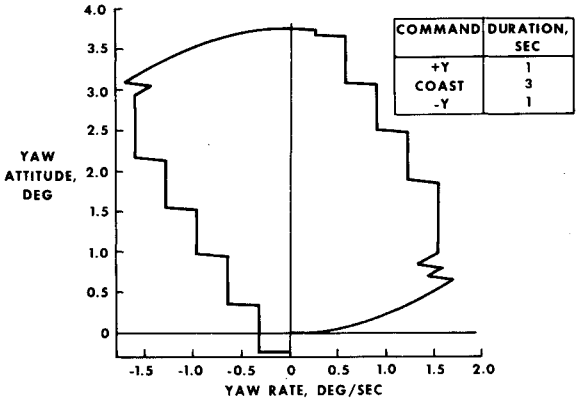

Fig. 8 Rate gyro response for typical maneuver: a) pilot/ASMU angular velocity; b) yaw attitude vs yaw rate.

Conclusions

The CMG and RG control system operating modes of the Skylab AMRV have been described in detail. Typical CMG and RG dynamics were analyzed in terms of an AMRV mass property configuration representing a 150-lb unsuited pilot with the ASMU. No propellant is used for normal operation or stabilization in the CMG mode, and the maximum rotation rate is 5°/sec per axis. In the RG mode attitude and attitude rate are maintained within limits of ± 4° and ± 2°/sec, respectively, with a maximum rotation rate of 20°/sec per axis. Translational maneuvering is identical in either mode, with linear velocities normally not exceeding 0.5 fps.

References

[1] Whitsett, C. E. and Cramer, P. S., "An Experimental Investigation of Attitude Control Systems for Astronaut Maneuvering Units," AIAA Paper 73-250, Washington, D.C., 1973.

[2] Meirovitch, L., *Methods of Analytical Dynamics,* McGraw-Hill, New York, 1970, Chap. 4.

[3] Tewell, J. R., "AMRV Astronaut Dynamics," Rept. MCR-70-33, Oct. 1970, Martin Marietta, Denver Division, Denver, Colo.

[4] Cramer, P. S., "ASMU Attitude Control System Design: M509 Experiment," Rept. MCR-29-486, prepared under Contract NAS9-0339, Aug. 1969, Martin Marietta, Denver Division, Denver, Colo.

[5] Cramer, P. S. and Josephson, J. T., "Attitude Control of an Astronaut by Backpack-Mounted Control Moment Gyros," Rept. TM-1640-27-69, Feb. 1969, Martin Marietta, Denver Division, Denver, Colo.

[6] Barker, W. F., "Detail Design Summary for Experiment M509," Rept. MCR-70-289, prepared under contract NAS9-9339, Nov. 1970, Martin Marietta, Denver Division, Denver, Colo.

[7] Greenwood, D. T., *Principles of Dynamics,* Prentice-Hall, Englewood Cliffs, N.J., 1965, Chap. 3.